O_3 fast and simple treatment-enhanced p-doped in Spiro-MeOTAD for CH_3NH_3I vapor-assisted processed $CH_3NH_3PbI_3$ perovskite solar cells*

En-Dong Jia(贾恩东)[1,2], Xi Lou(娄茜)[1,3], Chun-Lan Zhou(周春兰)[1,2,†], Wei-Chang Hao(郝维昌)[3,‡], and Wen-Jing Wang(王文静)[1,2]

[1] *The Key Laboratory of Solar Thermal Energy and Photovoltaic System, Institute of Electrical Engineering, Chinese Academy of Sciences, Beijing* 100190, *China*

[2] *University of Chinese Academy of Sciences (UCAS), Beijing* 100049, *China*

[3] *Department of Physics and Key Laboratory of Micro-nano Measurement, Manipulation and Physics, Beihang University, Beijing* 100191, *China*

(Received 19 December 2016; revised manuscript received 10 February 2017; published online 20 April 2017)

We demonstrate a simple and fast post-deposition treatment with high process compatibility on the hole transport material (HTM) Spiro-MeOTAD in vapor-assisted solution processed methylammonium lead triiodide ($CH_3NH_3PbI_3$)-based solar cells. The prepared Co-doped p-type Spiro-MeOTAD films are treated by O_3 at room temperature for 5 min, 10 min, and 20 min, respectively, prior to the deposition of the metal electrodes. Compared with the traditional oxidation of Spiro-MeOTAD films overnight in dry air, our fast O_3 treatment of HTM at room temperature only needs just 10 min, and a relative 40.3% increment in the power conversion efficiency is observed with respect to the result of without-treated perovskite solar cells. This improvement of efficiency is mainly attributed to the obvious increase of the fill factor and short-circuit current density, despite a slight decrease in the open-circuit voltage. Ultraviolet photoelectron spectroscopy (UPS) and Hall effect measurement method are employed in our study to determine the changes of properties after O_3 treatment in HTM. It is found that after the HTM is exposed to O_3, its p-type doping level is enhanced. The enhancement of conductivity and Hall mobility of the film, resulting from the improvement in p-doping level of HTM, leads to better performances of perovskite solar cells. Best power conversion efficiencies (PCEs) of 13.05% and 16.39% are achieved with most properly optimized HTM via CH_3NH_3I vapor-assisted method and traditional single-step method respectively.

Keywords: perovskite solar cells, Spiro-MeOTAD, simple, O_3 treatment

PACS: 88.40.H–, 88.40.hj **DOI:** 10.1088/1674-1056/26/6/068803

1. Introduction

Organometal halide perovskite solar cells are dramatically emerging as one of the most competitive solar technologies and revolutionizing the field of photovoltaics.[1–4] With desirable physical properties including broadly tunable bandgaps,[5] high absorption coefficients,[6] high carrier mobilities,[7] extremely long carrier diffusion lengths,[8,9] and good crystallinity,[10,11] organometal halide perovskite materials have been demonstrated to be excellent photovoltaic materials. Since the first version of the perovskite solar cell based on the sensitizer concept in 2009,[12] the power conversion efficiencies (PCEs) of perovskite-based devices have been enhanced from 3.8%[12] to 22% or more.[13] With the continuous development of the perovskite solar cells, this photovoltaic technology will achieve economic feasibility in the near future.

The common device structure of perovskite solar cells consists of a transparent conductive substrate, a compact TiO_2 hole-blocking layer, an organolead halide perovskite light-absorption layer combined with a porous scaffold, a hole transporting layer, and a metal counter electrode. Studies have mainly focused on hole-blocking layer optimization,[14] scaffold layers design,[10,15] high quality perovskite film formation methodologies,[16,17] alternative device structure,[18,19] and inherent mechanisms.[9,20,21] Hole transport material (HTM), as one of the key components in perovskite solar cells, separates photo-excited electron–hole pairs and transports the holes to the external circuit.[22] Therefore, the performance of perovskite solar cells is highly dependent on the properties of HTM. The 2,2',7,7'-tetrakis (N,N-di-p-methoxyphenylamine)-9,9' -spirobifluorene (Spiro-MeOTAD) is the most widely used and the best hole transport material in performance. Because of the high resistivity of the pristine Spiro-MeOTAD, additives like lithium bis (trifluoromethanesulfonyl) imide (Li-TFSI) and 4-tert-butylpyridine (t-BP) are used to dope (p-type) Spiro-MeOTAD to improve its transport property.[23] Among the published reports one adoptable strategy to further enhance its transport property is the oxi-

*Project supported by the National Natural Science Foundation of China (Grant Nos. 51472016 and 51272015).

†Corresponding author. E-mail: chunlzhou@gmail.com

‡Corresponding author. E-mail: whao@buaa.edu.cn

© 2017 Chinese Physical Society and IOP Publishing Ltd

dation process of Spiro-MeOTAD, such as annealing in dry O_2 for more than 10 h at 65 °C[24] and in air over night at room temperature[25] to improve the performance of the device. However, this time consuming process results in less cost-effectiveness.

In the present work, we investigate the $CH_3NH_3PbI_3$-based device with a structure of glass/fluorine-doped tin oxide (FTO)/TiO_2 compact layer/mesoporous TiO_2layer/ $CH_3NH_3PbI_3$/Co-doped p-type Spiro-MeOTAD/silver (Ag). The perovskite films are prepared via vapor-assisted solution processed deposition method.[26] The HTM films are treated in dry O_3 at room temperature for 3 different lengths of time: 5 min, 10 min, and 20 min, before evaporating Ag metal contact. The control samples are completely fabricated without O_3 treatment. It is observed that the performances of $CH_3NH_3PbI_3$-based devices are strongly affected by the O_3 treatment of the films, which leads to a substantial increase in the PCE of the device with the significant increase of the fill factor and current density. The processing conditions and corresponding results will be discussed in detail.

2. Experiment

$CH_3NH_3PbI_3$-based perovskite solar cells were fabricated under ambient condition. The x-ray diffraction (XRD), scanning electron microscope (SEM), UV-visible spectroscopy, ultraviolet photoelectron spectroscopy (UPS) and Hall effect measurement are used to characterize the material; I-V measurement is used to determine the photovoltaic performance of device.

2.1. Solar cell fabrication

The 35 mm ×35 mm square substrates, fluorine-doped tin oxide coated glasses (10 Ω/sq), were cleaned by ultrasonication in a detergent diluted washing solution, rinsed with deionized water and ethanol, dried in nitrogen, and then treated under O_3/ultraviolet for 30 min.

The clean FTO glasses were coated with 0.15-M and 0.3-M titanium diisopropoxide bis (acetylacetonate) at 3000 rpm for 30 s subsequently. After being heated on a hotplate at 125 °C for 15 min, the coated substrates were annealed in an oven at 550 °C for 30 min in air. The substrates were treated in 0.05-M $TiCl_4$ aqueous solution at 70 °C for 30 min and rinsed with deionized water, followed by being annealed at 550 °C for 20 min in air to form a compact n-type layer of TiO_2 (c-TiO_2).

Mesoporous TiO_2 films were deposited on the substrates by spin coating TiO_2 paste at 3000 rpm for 30 s, followed by being heated on a hotplate at 125 °C for 15 min and annealed at 550 °C for 30 min in air subsequently to form a layer of mesoporous TiO_2 (mp-TiO_2). The FTO/c-TiO_2/mp-TiO_2 substrates were preserved in nitrogen at 80 °C for 15 h.

The 460-mg/ml precursor of PbI_2 solution was prepared by dissolving PbI_2 into DMF, then heated to form clean yellow and clear solution. The PbI_2 solution in DMF was spin-coated on the FTO/c-TiO_2/ mp-TiO_2 substrates at 5000 rpm. for 10 s, and dried at 100 °C for 15 min. CH_3NH_3I powder was spread out around the PbI_2 coated substrates with a petri dish covering on the top, and heated at 120 °C for the desired time to form perovskite films. After cooling down, the as-prepared perovskite films were washed with isopropanol, dried and annealed at 80 °C for 30 min.

The perovskite films were coated with the HTM (Co-doped p-type Spiro-MeOTAD) by using the spin-coating method at 2000 rpm for 20 s. The spin-coated Spiro-MeOTAD films were treated with O_3, respectively, for 5 min, 10 min, and 20 min as shown in Fig. 1. Soda-lime glass would prevent UV light from irradiating the sample surface but allow O_3 to treat it. A sample without O_3 treatment was also prepared for comparison. The space for the UVO-treatment is about 0.5 M (length)×0.5 M (width) ×0.2 M (height). When the UVO treatment was proceeding, the space should avoid circulation of air.

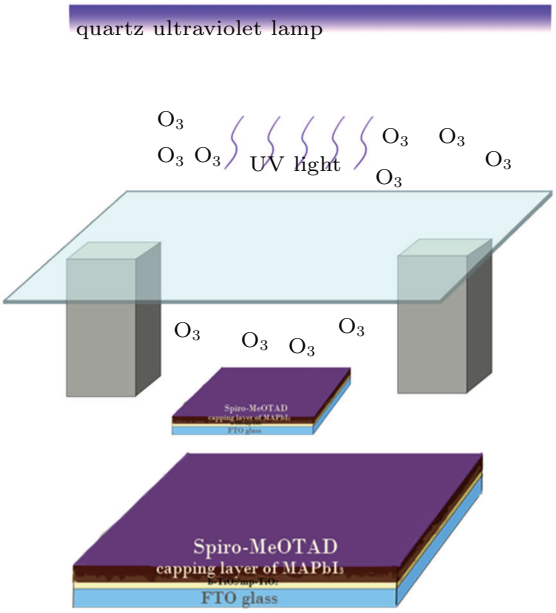


Fig. 1. (color online) Schematic procedure for the fast O_3 treatment to Spiro-MeOTAD films. Soda-lime glass excludes the direct UV rays.

Finally, the counter electrode was deposited by thermal evaporation of silver under a vacuum of 5×10^{-5} Torr (1 Torr = 1.33322×10^2 Pa). The active area was a bit larger than 0.07 cm^2 and was finally tested with a mask whose area was just 0.07 cm^2.

2.2. Characterization method

The *I–V* characteristics of the devices were measured by using the Keithley 2400 source meter under the calibrated solar simulator equipped with an AM 1.5 filter at 100 mW/cm^2. The *I–V* curves were obtained from the reverse scan at a

scan rate of 0.01 V·s^{-1} from 1.2 V to −0.2 V. The surface morphologies of the films were characterized by scanning electron microscopy (SEM) using the CARL ZEISS-SIGMA field emission scanning electron microscope. UV-visible spectroscopy was performed by using the Varian-Cary 500. X-ray diffraction (XRD) was determined by using the Bruker-D8 Advance in steps of 0.01° for 2θ from 10° to 60°.

Ultraviolet photoelectron spectroscopy (UPS) analysis was conducted by using Beijing synchrotron radiation light source. The charging effects were taken into account by referring the measured spectra to the binding energy peak of Au 4f at 84 eV. The conductivity and Hall mobility were recorded on the HL5500PC Hall Effect measurement system for Co-doped p-type Spiro-MeOTAD film deposited on a 0.5 cm×0.5 cm^2 square glass substrate.

3. Results and discussion

$CH_3NH_3PbI_3$-based solar cells are fabricated via vapor-assisted solution process.

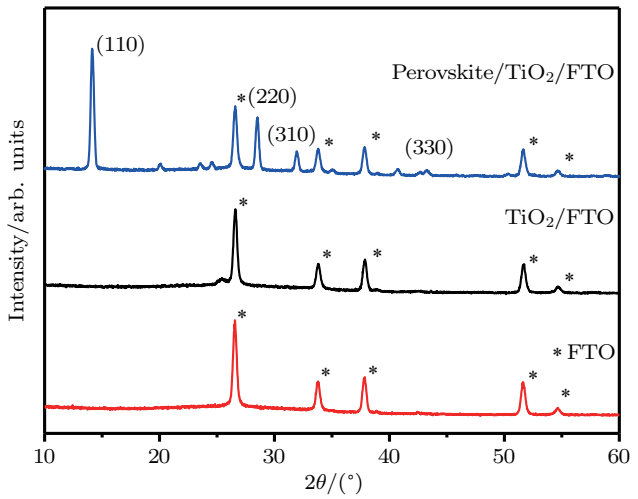


Fig. 2. (color online) XRD patterns of fluorine-doped tin oxide (FTO, red curve), c-TiO_2 and meso-TiO2 on FTO (FTO/TiO2, black curve), and metal organic halide perovskite (FTO/TiO_2/Perovskite, blue curve).

Figure 2 shows the corresponding XRD of the as-prepared $CH_3NH_3PbI_3$ film on FTO/TiO_2 substrate. It provides evidence for the high crystalline nature of our sample and shows the tetragonal perovskite pattern with peaks at 14.13°, 28.52°, 31.93°, 43.22°, corresponding to (110), (220), (310), and (330) respectively, which are in good agreement with previously reported results.[26,27] The broad absorption spectrum of $CH_3NH_3PbI_3$ is shown in Fig. 3, indicating the strong photon harvesting capability of the material over the spectral range from 400 nm to 800 nm, which is in agreement with the band gap of 1.5 eV for $CH_3NH_3PbI_3$. The morphologies of the samples have been investigated by scanning electron microscopy (SEM) and the images of typical films are presented in Fig. 3. From the top-view image of $CH_3NH_3PbI_3$ formed on meso-TiO_2 layer, crystalline domains of perovskite with grain size in a range from 200 nm to 400 nm with good surface coverage are observed. As incomplete coverage of perovskite results in undesired shunting paths and minimizes light absorption in solar cells, high surface coverage is important for high performance devices.[24] In addition, crystals with large grain size and good crystalline quality are shown to be favorable for charge transport by suppressing charge trapping during solar cell operation. Thus, they are preferable for the development of high performance devices.[28]

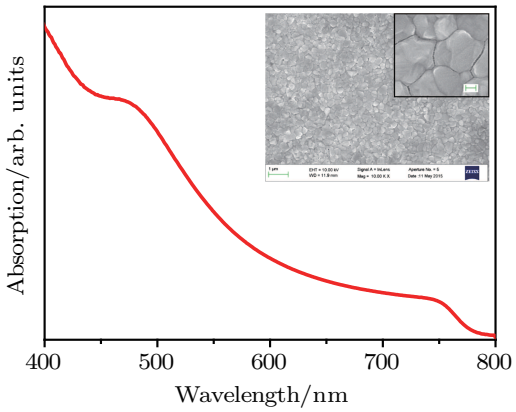


Fig. 3. (color online) Absorption spectrum of $CH_3NH_3PbI_3$ film and top-view SEM images for the sample of FTO/TiO_2/$CH_3NH_3PbI_3$. (Insert image with higher resolution, scale bar: 100 nm).

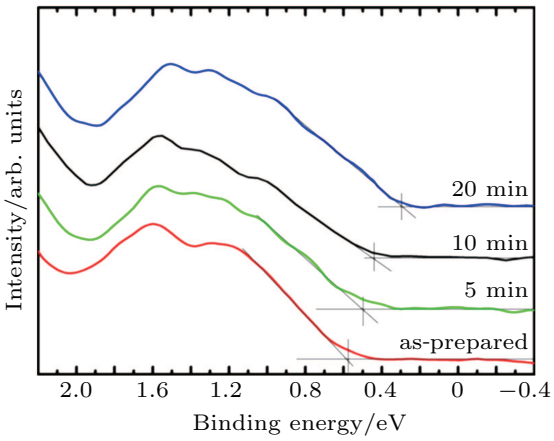


Fig. 4. (color online) UPS corresponding to the HOMO region of the as-prepared sample and samples with different O_3 treatment times.

The changes of the electronic properties of the as prepared Spiro-MeOTAD film and film after O_3 exposure are probed by UPS with a synchrotron radiation light source. As can be seen in Fig. 4 the leading edge of the highest occupied molecular orbital (HOMO) with respect to the Fermi level for the as-prepared sample is at 0.58 eV. After the first 5-min exposure to O_3, the HOMO level of the Spiro-MeOTAD film shows a slight shift toward low binding energy settling at 0.49 eV, illustrated by the green curve. An additional 5-min O_3 treatment induces further shift, bringing the HOMO leading edge to −0.44 eV. With a total treatment time of 20 min, the HOMO shows an obvious shift with the leading edges at

−0.3 eV, illustrated by the blue curve. This is indicative of improved p-type doping level of Spiro-MeOTAD film with the increase of the time of exposure to O_3. Oxygen has been reported to be essential for the doping mechanism of Spiro-MeOTAD. Cappel *et al.* suggested that the oxygen acts as an electron accepter in an *in situ* oxidation of Spiro-MeOTAD in solid state dye-sensitized solar cells.[29] Similarly, ozone as a powerful oxidant can efficiently oxidize Spiro-MeOTAD and enhance its doping level.

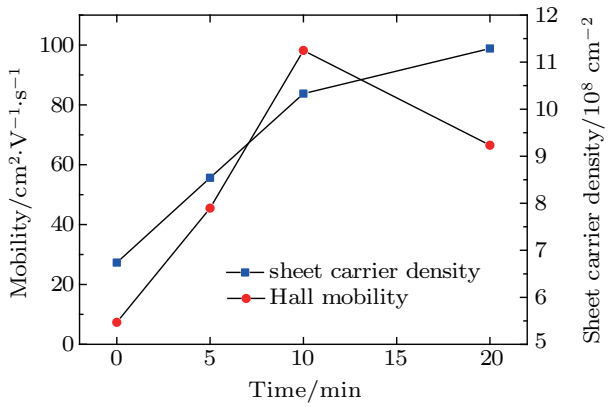


Fig. 5. (color online) Time-dependent carrier mobility and sheet carrier density of the spin-coated Spiro-MeOTAD film on glass substrate.

To record the carrier density, Hall mobility and conductivity of the Co-doped p-type Spiro-MeOTAD film, the Hall effect measurement is adopted. The sample is obtained by spinning on 0.5 cm×0.5 cm square glass at 2000 rpm for 20 s. The thickness of the film is 500 nm. Hall mobility (μ), sheet carrier density (N_s), and conductivity (σ) of the as-prepared Spiro-MeOTAD film are measured at room temperature by the van der Pauw method. This sample is re-measured several times after O_3 treatment for 5 min, 10 min, and 20 min. Hall mobility and sheet carrier density are shown in Fig. 5. Longer O_3 treatment time results in larger carrier density. As O_3 treatment enhances the p-type doping level in Spiro-MeOTAD film as shown in Fig. 4 it is easy to understand the increased trend of carrier concentration with the increase of holes as the dominant carriers. Additionally, the hole mobility of Spiro-MeOTAD film increases with the sheet charge density increasing from 6.7×10^8 cm^{-2} to 1×10^9 cm^{-2} and reaches the peak at 10-min O_3-treatment. This trend is consistent with previously reported results of charge-density-dependent mobility for this material, while the exact values of hole mobility and charge density differ somehow from the values of previously reported results because of the differences in sample structure and measuring method.[30] However, as the hole–hole scattering may suppress the mobility, a decrease in hole mobility can be observed from Fig. 5 with the further increase of the charge density when additional O_3 treatment is performed. The conductivity originating from the electron charge is shown in Fig. 6. The variety of conductivity is generally coincident with that of hole mobility, showing a strong dependence on the O_3 exposure time. Similar result of reduction in the resistance of the Spiro-MeOTAD layer after annealing in O_2 ambient at 65 °C for 12 h has also been reported previously.[24] As a result, the best mobility and conductivity of Spiro-MeOTAD film are obtained with 10 min O_3 treatment.

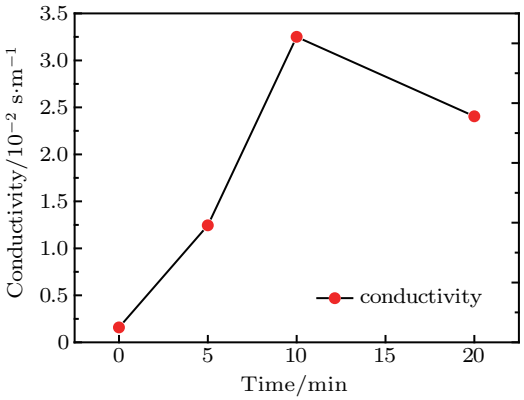


Fig. 6. (color online) Conductivity of the spin-coated Spiro-MeOTAD film on glass substrate versus O_3 treatment time.

To further confirm the effect of O_3 treatment, we examine the exposure-time-dependent photovoltaic performance of $CH_3NH_3PbI_3$-based solar cells employing Spiro-MeOTAD as HTM with different exposure times. *J–V* curves of average performance devices as representative devices are shown in Fig. 7(d). The relationships of serial resistance (R_s), fill factor (FF), short-circuit photocurrent density (J_{sc}), open-circuit voltage (V_{oc}), and efficiency (η) with O_3 treatment are presented in Figs. 6 and 7(a)–7(d). In comparison with the control group, devices with O_3 treatment yields better performance with the increase of J_{sc} and FF, despite a slight decrease in V_{oc}. As shown in Fig. 6, the average series resistance (R_s) of device without O_3 treatment is 20.2 Ω. It substantially decreases to 11.8 Ω after 5-min O_3 treatment. With an additional 5 min treatment, R_s drops to the bottom of 8.1 Ω. Then, it increases slightly to 9.0 Ω with a total of 20-min treatment. It is well known that the R_s represents the total resistance of the cell and is a resultant resistance of the active and interfacial layer resistances, electrode resistances, and the various contact and interconnect resistances.[31] Combining with results from Hall effect measurement, it is reasonable to believe that the conductivity and mobility increase of hole transport layer increase the series resistance. R_s can have a pronounced effect on the solar cell fill factor (FF), and FF is often the dominant parameter determining the power conversion efficiency. The lower R_s enables a large FF.[14] In Fig. 7(a), average FF substantially increases from 45.48% without O_3 treatment to 53.54% with 5-min treatment, corresponding to the opposite trend of R_s. An additional 5-min treatment induces an increase, obtaining FF of 57.67%, while the further increase of

the O_3 treatment time to 20 min results in a reduction in FF. According to Fig. 7(b), short-circuit photocurrent density (J_{sc}) shares the same trend with FF. Devices with O_3 treatment yields higher J_{sc} than devices without O_3 treatment. The improved J_{sc} suggests that the carrier collection efficiency across the perovskite/ Spiro-MeOTAD interface is improved. This may result from the hole mobility enhancement, thus improving the hole transport in HTM. In addition, 10-min exposure achieves optimization with J_{sc} of 18.59 mA/cm^2 on average, while less or further exposure induced a decline in J_{sc}, consistent with the result of hole mobility. The open circuit voltage (V_{oc}) decreases slightly with O_3 treatment increasing, but the reason is not clear. As a result, the average conversion efficiency of Spiro–MeOTAD film increases from 6.7% without O_3 treatment to 9.4% with 10-min oxidation process, corresponding to 40.3% increment. The best performance device achieves η of 13.05%, with $V_{oc} = 0.99$ V, $J_{sc} = 21.64$ mA/cm^2, $FF = 60.91\%$ as shown in Fig. 8(a). It is a remarkable fact that the value of η reaches 13% via CH_3NH_3I vapor-assisted method in ambient air. We also fabricate perovskite solar cells in a strictly controlled (ppm < 1 for both O_3 and H_2O) glove box via traditional single step.[32–37] The best performance of device achieves the η value of 16.39%, with $V_{oc} = 1.1$ V, $J_{sc} = 19.96$ mA/cm^2, $FF = 74.49\%$ as shown in Fig. 8(b). In strictly controlled atmosphere the quality of perovskite film can be much better than in ambient air. We do not discuss more details of this point because the oxidation and doping level of spiro-MeOTAD under O_3 are the key points of this article.

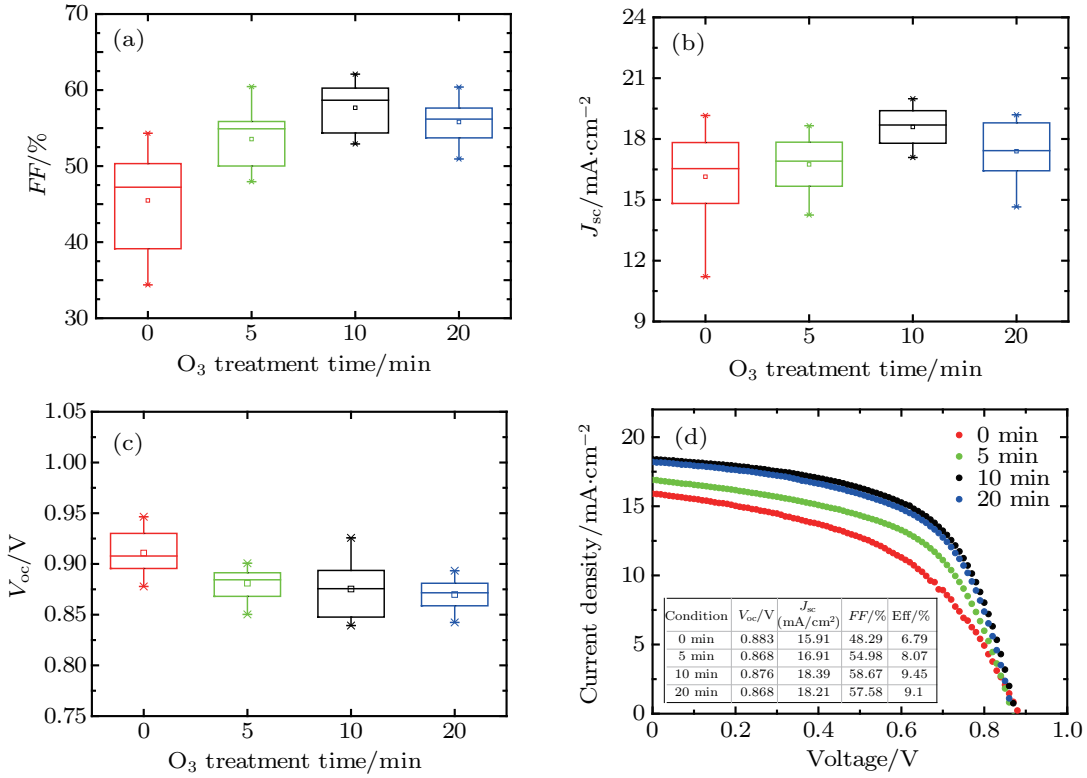


Fig. 7. (color online) The average values of photovoltaic parameters obtained from I–V measurements for $CH_3NH_3PbI_3$-based solar cells with different O_3 treatment times. (a) FF, (b) J_{sc}, (c) V_{oc}, and (d) J–V curves of average performance devices with different O_3 treatment times.

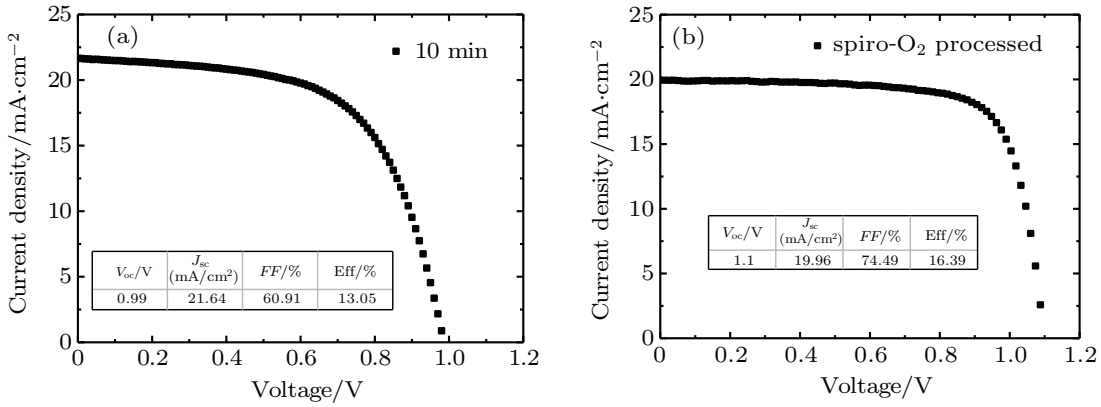


Fig. 8. J–V curve of the best performance device with the optimized O_3 treatment time via (a) vapor-assisted in air and (b) single-step in glove box.

4. Conclusions

In this work, O_3 is adopted to treat co-doped p-type Spiro-MeOTAD film at room temperature before evaporating Ag metal contact when fabricating $CH_3NH_3PbI_3$-based perovskite solar cells under ambient condition. The O_3 treatment procedure enhances p-doping level in this hole transport material which is evidenced by the HOMO level approaching Fermi level after O_3 treatment. This leads to the increase in the carrier density, improvement in the carrier mobility and optimization in conductivity of Spiro-MeOTAD, which is confirmed by Hall effect measurement. Results suggest that the enhancements in the conductivity and carrier mobility lead to better device performance and 10-min treatment turned out to be favorable for the optimization, thus achieving a 40.3% increment in the PCEs: an averaged enhancement is 9.4%. The values of η reach, respectively, 13.05% in ambient air via CH_3NH_3I vapor-assisted method and 16.39% in glove box via traditional single-step method, indicating that the device achieves the best performance. This presents a short-time and effective process to improve the efficiency of organometal halide perovskite solar cells

References

[1] Snaith H J 2013 *J. Phys. Chem. Lett.* **4** 3623

[2] Green M A, Ho-Baillie A and Snaith H J 2014 *Nat. Photon.* **8** 506

[3] Kim H S, Im S H and Park N G 2014 *J. Phys. Chem. C* **118** 5615

[4] Boix P P, Nonomura K, Mathews N and Mhaisalkar S G 2014 *Mater. Today* **17** 16

[5] Eperon G E, Stranks S D, Menelaou C, Johnston M B, Herz L M and Snaith H J 2014 *Energy Environ. Sci.* **7** 982

[6] Im J H, Lee C R, Lee J W, Park S W and Park N G 2011 *Nanoscale* **3** 4088

[7] Mitzi D B 1999 *Progress in Inorganic Chemistry*, Vol. 48, Karlin K D ed. (New York: John Wiley & Sons Inc.) pp. 1–121

[8] Stranks S D, Eperon G E, Grancini G, Menelaou C, Alcocer M J P, Leijtens T, Hertz L M, Petrozza A and Snaith H J 2013 *Science* **342** 341

[9] Xing G C, Mathews N, Sun S Y, Lim S S, Lam Y M, Gratzel M, Mhaisalkar S and Sum T C 2013 *Science* **342** 344

[10] Lee M M, Teuscher J, Miyasaka T, Murakami T N and Snaith H J 2012 *Science* **338** 643

[11] Stoumpos C C, Malliakas C D and Kanatzidis M G 2013 *Inorg. Chem.* 52 pp. 9019–9038

[12] Kojima A, Teshima K, Shirai Y and Miyasaka T 2009 *J. Am. Chem. Soc.* **131** 6050

[13] Yang W S, Noh J H, Jeon N J, Kim Y C, Ryu S, Seo J and Seok S 2015 *Science* **348** 1234

[14] Wu Y, Yang X, Chen H, Zhang K, Qin C, Liu J, Peng W Q, Islam A, Bi E B and Ye F 2014 *Appl. Phys. Express* **7** 052301

[15] Ball J M, Lee M M, Hey A and Snaith H J 2013 *Energy Environ. Sci.* **6** 1739

[16] Im J H, Jang I H, Pellet N, Gratzel M and Park N G 2014 *Nat. Nanotechnol.* **9** 927

[17] Nie W, Tsai H, Asadpour R, Blancon J C, Neukirch A J and Gupta G 2015 *Science* **347** 522

[18] Abu Laban W and Etgar L 2013 *Energy Environ. Sci.* **6** 3249

[19] Liu D, Yang J and Kelly T L 2014 *J. Am. Chem. Soc.* **136** 17116

[20] Gonzalez-Pedro V, Juarez-Perez E J, Arsyad W S, Barea E M, Fabregat-Santiago F and Mora-Sero I 2014 *Nano. Lett.* **14** 888

[21] Sum T C and Mathews N 2014 *Energy Environ. Sci.* **7** 2518

[22] Zhang H, Shi Y T, Yan F, Wang L, Wang K, Xing Y J, Donga Q S and Ma T L 2014 *Chem. Commun.* **50** 5020

[23] Schölin R, Karlsson M H, Eriksson S K, Siegbahn H, Johansson E M J and Rensmo H 2012 *J. Phys. Chem. C* **116** 26300

[24] Ren Z W, Ng A, Shen Q, Gokkaya H C, Wang J, Yang L J, Yiu W K, Bai G X, Djurisic A B and Leung W W F 2014 *Sci. Rep.* **4** 6752

[25] Chen H W, Sakai N, Ikegami M and Miyasaka T 2015 *J. Phys. Chem. Lett.* **6** 164

[26] Chen Q, Zhou H, Hong Z, Luo S, Duan H S, Wang H H, Liu Y S, Li G and Yang Y 2014 *J. Am. Chem. Soc.* **136** 622

[27] Baikie T, Fang Y, Kadro J M, Schreyer M, Wei F, Mhaisalkar S G, Graetzel M and White T J 2013 *J. Mater. Chem. A* **1** 5628

[28] Nie W Y, Tsai H H, Asadpour R, Blancon J C, Neukirch A J, Gupta G, Crochet J J, Chhowalla M, Tretiak S and Alam M A 2015 *Science* **347** 522

[29] Cappel U B, Daeneke T and Bach U 2012 *Nano. Lett.* **12** 4925

[30] Leijtens T, Lim J, Teuscher J, Park T and Snaith H J 2013 *Adv. Mater.* **25** 3227

[31] Servaites J D, Yeganeh S, Marks T J and Ratner M A 2010 *Adv. Funct. Mater.* **20** 97

[32] Wang T Y, Cheng J W, Wu G X and Li M C 2016 *Sci. China-Mater.* **59** 703

[33] Song D D, Cui P, Wang T Y, Wei D, Li M C, Cao F H, Yue X P, Fu P F, Li Y Y and He Y 2015 *J. Phys. Chem. C* **119** 22812

[34] Song D D, Wei D, Cui P, Li M, Duan Z Q, Wang T Y, Ji J, Li Y Y, Jbengue J M, Li Y F, He Y, Trevor M and Park N G 2016 *J. Mater. Chem. A* **4** 6091

[35] Zhang Z R, Yue X P, Wei D, Li M C, Fu P F, Xie B X, Song D D and Li Y F 2015 *RSC Adv.* **5** 104606

[36] Wei D, Ji J, Song D D, Li M C, Cui P, Li Y Y, Mbengue J M, Zhou W J, Ning Z J and Park N G 2017 *J. Mater. Chem. A* **5** 1406

[37] Cui P, Fu P F, Wei D, Li M C, Song D D, Yue X P, Li Y Y, Zhang Z R, Li Y F and Mbengue J M 2015 *RSC Adv.* **5** 75622